https://doi.org/10.1016/j.jcsr.2020.106061


# Design-oriented model for circular F-STC stub columns subjected to axial compression

Tianxiang Xu[a,b], Jiepeng Liu[a,b,*], Tao Yu[c,d], Ying Guo[a,b]

[a] School of Civil Engineering, Chongqing University, Chongqing 400045, China

[b] Key Laboratory of New Technology for Construction of Cities in Mountain Area (Chongqing University), Ministry of Education, Chongqing 400045, China

[c] Department of Civil and Environmental Engineering, The Hong Kong Polytechnic University, Hung Hom, Kowloon, Hong Kong, China

[d] School of Civil, Mining and Environmental Engineering, Faculty of Engineering, University of Wollongong, Northfields Avenue, Wollongong, NSW 2522, Australia

**Abstract:** A fiber-reinforced polymer (FRP)-steel composite tubed concrete (F-STC) column is formed by wrapping FRP sheets around a steel tubed concrete column (STC). Both the strength and deformability of the core concrete are improved by the FRP-steel composite tube and the steel tube is prevented from corrosion. A number of studies have been conducted on the prediction of stress-strain behavior of FRP-confined concrete columns and steel tube-confined concrete columns. However, few models focus on the concrete under combined confinement of FRP and steel tube. This paper presents an analytical study on the design-oriented model for F-STC columns. To determine the confining stress, the stress distribution of steel tube was firstly analyzed and the equivalent stress was obtained. In addition, a strain efficiency factor was proposed for the prediction of rupture strain of FRP. Then the peak condition and ultimate condition of F-STC columns were investigated and related predicting models for the load bearing capacity and deformation were proposed. Finally, design-oriented models were proposed for F-STC columns with different types of axial load-strain curves and generally coincided well with the existing test results.

**Keywords:** FRP-steel composite tubed concrete; stub column; equivalent stress; strain efficiency factor; design-oriented model

***Corresponding author.**

**E-mail address:** liujp@cqu.edu.cn.

## 1 Introduction

Fiber reinforced polymer (FRP) is widely applied to retrofit existing buildings because of its advantages of high strength, light weight, good corrosion resistance, and good fatigue resistance [1-4]. But the relatively brittle post-peak behavior and complicated construction procedures limit its application to newly-built buildings.

Concrete filled steel tube (CFST) column has been recognized as an ideal kind of composite members to be applied to high-rise and large-span structures. This is because the confinement of outer steel tube can improve both the strength and ductility of the core concrete and the potential inward buckling of steel tube is also restricted by the core concrete [5-12]. However, the steel tube needs to be thick enough to avoid local buckling problem and the confinement of steel tube cannot be realized at the initial loading stage because of the delamination at the interface between the steel tube and concrete [9]. Tomii et al. [13] proposed a novel type of composite column termed the steel tubed concrete (STC) column. The steel tube in the STC column is discontinuous at the beam-column joint section and mainly provides lateral confinement for the core concrete. Without bearing

any direct axial load, the steel tube does not need to be too thick and the construction process of the joints is significantly simplified [14-15]. However, for both kinds of columns, the confinement of steel tube is limited for high strength concrete (HSC) and many measures need to be taken to avoid the corrosion of steel tube.

Combination of FRP sheets and STC column takes advantages of both FRP and STC columns, termed the FRP-steel composite tubed concrete (F-STC) column [16-20]. The outer FRP-steel composite tube is prefabricated at the factory and used as frameworks for the concrete pouring. The confining stress provided by the FRP-steel composite tube will enhance the strength and ductility of the core concrete, and the corrosion and buckling problems of steel tube are suppressed by FRP. In addition, existence of steel tube ensures relatively ductile post-peak behavior of F-STC columns. Extensive research work has been conducted on the axial behavior of FRP confined CFST (F-CFST) columns. The influences of the FRP layers [21-29], slenderness ratio of steel tube [28, 30-31], shape of steel tube [22], diameter-to-thickness ratio of steel tube [23-27], concrete strength [26, 29] on the axial behavior of FRP confined CFST columns were investigated. Predicted models for the axial stress-axial strain curves of FRP confined CFST columns were also proposed, including analysis-oriented models [29, 32-34] and design-oriented models [35-36]. Only a few papers, however, experimentally investigated the behavior of F-STC columns subjected to concentric load [16-20].

Preliminary studies have demonstrated that combination of FRP and steel tube significantly improved the strength and deformation capacity of core concrete. It is necessary to come up with design methods to promote the practical application of F-STC columns. However, to the best knowledge of the authors, only design-oriented model for F-CFST columns was proposed, which was not applicable to F-STC columns as the steel tube in F-STC columns did not bear any direct axial load. To develop an accurate design-oriented model for F-STC columns, a database was firstly assembled based on existing test results. The stress distribution of steel tube was analyzed and equivalent stress of steel tube was obtained. And strain efficiency factor was proposed to evaluate the rupture strain of FRP. Finally, based on investigations on the peak condition and ultimate condition of F-STC columns, design-oriented models were proposed for F-STC columns with different types of axial load-strain curves.

# 2 Experimental test databases

## 2.1 Limit of diameter-to-thickness ratio of steel tube

The diameter-to-thickness ratio of steel tube ($D/t_s$) is one of the key parameters that influence the behavior of CFST columns. On one hand, the strength of steel tube cannot be fully used if the $D/t_s$ is too small. On the other hand, if the $D/t_s$ is too large, the confinement of steel tube is not sufficient to improve the strength and ductility of core concrete, and the steel tube will be more susceptible to local buckling problem. According to Eurocode 4 [37], the influence of local buckling may be neglected provided that $D/t_s$ did not exceed $90\frac{235}{f_y}$ ($f_y$=the yield stress of steel tube). As for F-STC columns, no direct axial load is applied to the steel tube and the buckling problem of steel tube is further suppressed by both the concrete and FRP sheets. Therefore, it allows to adopt relatively thin-walled steel tube, resulting in lighter and more economical structures. The lower limit of $D/t_s$ of circular F-STC columns is obtained without consideration of the correction of steel tube strength, as shown in Eq. (1).

$$D/t_s \geq 90 \quad (1)$$

There is no explicit upper limit of $D/t_s$, however, confinement of steel tube and FRP should be sufficient to ensure that the core concrete can work together with longitudinal steel bars or steel shape, which means that the steel bars or steel shape should yield before specimens reach the peak load. Therefore, the calculated axial strain of F-STC columns at the peak load ($\varepsilon_{fc}^{c}$) should be larger than the yield strain of steel bars and steel shape ($\varepsilon_y$).

The database is assembled based on existing studies on the axial behavior of F-STC stub columns [16-20]. The results included in the database are chosen according to the limit of $D/t_s$ and the length to diameter ratio ($L/D \leq 3$). Details of specimens are summarized in Table 1, which covers the following information of F-STC columns: the geometric dimensions (diameter, $D$, and length, $L$); FRP properties given by the manufacturer (elastic modulus, $E_{frp}$, rupture strain, $\varepsilon_{fu}$, and thickness, $t_f$); properties of steel tube (yield stress, $f_y$, and thickness, $t_s$); concrete properties (cubic compressive strength, $f_{cu}$, and unconfined strength, $f_{co}$); measured transverse strain of FRP (strain at peak load, $\varepsilon_{fp}$, and rupture strain, $\varepsilon_{rupt}$); peak condition of specimens (peak bearing capacity, $N_p^e$, and corresponding axial deformation, $\delta_p^e$); and the ultimate condition of specimens (axial deformation at ultimate condition, $\delta_u^e$). $f_{co}$ is obtained according to the relationship between the cylinder characteristic strength and cubic characteristic strength shown in Eurocode 2 [38], in addition, the cubic characteristic strength is determined by linear extension of the coefficients in Chinese code GB-50010-2010 [39]. As presented in Table 1, the cubic strength of concrete ($f_{cu}$) varies from 57 MPa to 105 MPa and $D/t_s$ varies from 87 to 172.

104

Table 1 Summary of details of test specimens

| Paper | Specimen Numbers | Specimen Dimensions | | FRP Properties | | | Steel Properties | | Concrete Properties | | Transverse Strain of FRP | | Peak Condition | | Ultimate Condition |
|---|---|---|---|---|---|---|---|---|---|---|---|---|---|---|---|
| | | $D$ (mm) | $L$ (mm) | $E_{frp}$ (GPa) | $\varepsilon_{fu}$ (με) | $t_f$ (mm) | $f_y$ (MPa) | $t_s$ (mm) | $f_{cu}$ (MPa) | $f_{co}$ (MPa) | $\varepsilon_{fp}$ (με) | $\varepsilon_{rupt}$ (με) | $N_p^e$ (kN) | $\delta_p^e$ (mm) | $\delta_u^e$ (mm) |
| Guo et al. [16] | S1[a] | 200 | 600 | 235 | 16200 | 0.334 | 264.3 | 2 | 57.1 | 44 | 9278 | 9278 | 2633 | 8.54 | 8.54 |
| Guo et al. [16] | S2[a] | 200 | 600 | 235 | 16200 | 0.334 | 264.3 | 2 | 57.1 | 44 | 9004 | 9004 | 2755 | 9.47 | 9.47 |
| Guo et al. [16] | S3[a] | 200 | 600 | 235 | 16200 | 0.334 | 264.3 | 2 | 66.8 | 52.7 | 9169 | 9169 | 3048 | 7.95 | 7.95 |
| Guo et al. [16] | S4[a] | 200 | 600 | 235 | 16200 | 0.334 | 264.3 | 2 | 66.8 | 52.7 | 10111 | 10111 | 3017 | 4.86 | 4.86 |
| Guo et al. [16] | S5[b] | 260 | 780 | 235 | 16200 | 0.334 | 264.3 | 2 | 57.1 | 44 | 3667 | 8629 | 3736 | 4.92 | 8.67 |
| Guo et al. [16] | S6[b] | 260 | 780 | 235 | 16200 | 0.334 | 264.3 | 2 | 57.1 | 44 | 4176 | 8463 | 3610 | 4.40 | 9.39 |
| Guo et al. [16] | S7[c] | 260 | 780 | 235 | 16200 | 0.334 | 264.3 | 2 | 66.8 | 52.7 | 4168 | 9857 | 4345 | 4.8 | 8.44 |
| Guo et al. [16] | S8[c] | 260 | 780 | 235 | 16200 | 0.334 | 264.3 | 2 | 66.8 | 52.7 | 1602 | 2245 | 3847 | 4.29 | 7.61 |
| Liu et al. [17] | S9[a] | 200 | 600 | 235 | 16200 | 0.334 | 264.3 | 2 | 57.1 | 44 | 9315 | 9315 | 2607 | 10.55 | 10.55 |
| Liu et al. [17] | S10[a] | 200 | 600 | 235 | 16200 | 0.668 | 264.3 | 2 | 57.1 | 44 | 10975 | 10975 | 3456 | 14.18 | 14.18 |
| Liu et al. [17] | S11[a] | 200 | 600 | 235 | 16200 | 0.668 | 264.3 | 2 | 57.1 | 44 | 11338 | 11338 | 3083 | 11.34 | 11.34 |
| Liu et al. [17] | S12[a] | 200 | 600 | 235 | 16200 | 0.668 | 264.3 | 2 | 57.1 | 44 | 9723 | 9723 | 3327 | 12.12 | 12.12 |
| Liu et al. [17] | S13[a] | 200 | 600 | 235 | 16200 | 0.334 | 264.3 | 2 | 66.8 | 52.7 | — | — | 3190 | 7.98 | 7.98 |
| Liu et al. [17] | S14[a] | 200 | 600 | 235 | 16200 | 0.668 | 264.3 | 2 | 66.8 | 52.7 | 9182 | 9182 | 3846 | 10.17 | 10.17 |
| Liu et al. [17] | S15[a] | 200 | 600 | 235 | 16200 | 0.668 | 264.3 | 2 | 66.8 | 52.7 | 8957 | 8957 | 3469 | 9.42 | 9.42 |
| Liu et al. [17] | S16[a] | 200 | 600 | 235 | 16200 | 0.668 | 264.3 | 2 | 66.8 | 52.7 | 10513 | 10513 | 3776 | 10.32 | 10.32 |
| Liu et al. [17] | S17[b] | 260 | 780 | 235 | 16200 | 0.334 | 264.3 | 2 | 57.1 | 44 | 1965 | 8393 | 3360 | 4.52 | 9.30 |
| Liu et al. [17] | S18[a] | 260 | 780 | 235 | 16200 | 0.668 | 264.3 | 2 | 57.1 | 44 | 6799 | 6799 | 4780 | 15.52 | 15.52 |
| Liu et al. [17] | S19[a] | 260 | 780 | 235 | 16200 | 0.668 | 264.3 | 2 | 57.1 | 44 | 4800 | 4800 | 4050 | 11.26 | 11.26 |
| Liu et al. [17] | S20[a] | 260 | 780 | 235 | 16200 | 0.668 | 264.3 | 2 | 57.1 | 44 | 10157 | 10157 | 4757 | 13.79 | 13.79 |

| | | | | | | | | | | | | | | | |
|---|---|---|---|---|---|---|---|---|---|---|---|---|---|---|---|
| Liu et al. [17] | S21[c] | 260 | 780 | 235 | 16200 | 0.334 | 264.3 | 2 | 66.8 | 52.7 | 3001 | 3546 | 4321 | 4.84 | 7.42 |
| Liu et al. [17] | S22[a] | 260 | 780 | 235 | 16200 | 0.668 | 264.3 | 2 | 66.8 | 52.7 | 7278 | 7278 | 4711 | 9.61 | 9.61 |
| Liu et al. [17] | S23[a] | 260 | 780 | 235 | 16200 | 0.668 | 264.3 | 2 | 66.8 | 52.7 | 9668 | 9668 | 5374 | 11.75 | 11.75 |
| Liu et al. [17] | S24[a] | 260 | 780 | 235 | 16200 | 0.668 | 264.3 | 2 | 66.8 | 52.7 | 9869 | 9869 | 5131 | 13.68 | 13.68 |
| Guo et al. [18] | S25[a] | 260 | 780 | 246 | 17100 | 0.334 | 299 | 2 | 76.5 | 60.8 | 10169 | 10169 | 4788 | 6.41 | 6.41 |
| Guo et al. [18] | S26[a] | 260 | 780 | 246 | 17100 | 0.334 | 299 | 2 | 76.5 | 60.8 | 10664 | 10664 | 4779 | 8.37 | 8.37 |
| Guo et al. [18] | S27[a] | 260 | 780 | 246 | 17100 | 0.334 | 299 | 2 | 76.5 | 60.8 | 9212 | 9212 | 4677 | 5.36 | 5.36 |
| Guo et al. [18] | S28[a] | 260 | 780 | 246 | 17100 | 0.668 | 299 | 2 | 76.5 | 60.8 | 10828 | 10828 | 5890 | 10.20 | 10.20 |
| Guo et al. [18] | S29[a] | 260 | 780 | 246 | 17100 | 0.668 | 299 | 2 | 76.5 | 60.8 | 8397 | 8397 | 5596 | 9.00 | 9.00 |
| Guo et al. [18] | S30[a] | 260 | 780 | 246 | 17100 | 0.668 | 299 | 2 | 76.5 | 60.8 | 8602 | 8602 | 5340 | 5.50 | 5.50 |
| Liu et al. [19] | S31[a] | 260 | 780 | 246 | 17100 | 0.334 | 299 | 2 | 72.5 | 58.4 | 10862 | 10862 | 4494 | 5.80 | 5.80 |
| Liu et al. [19] | S32[a] | 260 | 780 | 246 | 17100 | 0.334 | 299 | 2 | 72.5 | 58.4 | 13257 | 13257 | 4747 | 6.57 | 6.57 |
| Liu et al. [19] | S33[a] | 260 | 780 | 246 | 17100 | 0.334 | 299 | 2 | 72.5 | 58.4 | 11863 | 11863 | 4581 | 7.02 | 7.02 |
| Liu et al. [19] | S34[a] | 260 | 780 | 246 | 17100 | 0.668 | 299 | 2 | 72.5 | 58.4 | 7100 | 7100 | 5567 | 8.31 | 8.31 |
| Liu et al. [19] | S35[a] | 260 | 780 | 246 | 17100 | 0.668 | 299 | 2 | 72.5 | 58.4 | 8718 | 8718 | 5419 | 7.75 | 7.75 |
| Liu et al. [19] | S36[a] | 260 | 780 | 246 | 17100 | 0.668 | 299 | 2 | 72.5 | 58.4 | 15355 | 15355 | 5558 | 11.13 | 11.13 |
| Liu et al. [19] | S37[c] | 200 | 600 | 246 | 17100 | 0.334 | 299 | 2 | 105 | 80.6 | 2568 | 6332 | 4127 | 2.36 | 3.76 |
| Liu et al. [19] | S38[c] | 200 | 600 | 246 | 17100 | 0.334 | 299 | 2 | 105 | 80.6 | 5443 | 9392 | 4230 | 2.33 | 3.44 |
| Liu et al. [19] | S39[c] | 200 | 600 | 246 | 17100 | 0.334 | 299 | 2 | 105 | 80.6 | 2292 | 9068 | 4212 | 2.18 | 4.04 |
| Liu et al. [19] | S40[a] | 200 | 600 | 246 | 17100 | 0.668 | 299 | 2 | 105 | 80.6 | 7442 | 7442 | 4523 | 4.89 | 4.89 |
| Liu et al. [19] | S41[a] | 200 | 600 | 246 | 17100 | 0.668 | 299 | 2 | 105 | 80.6 | 11792 | 11792 | 4939 | 5.21 | 5.21 |
| Liu et al. [19] | S42[a] | 200 | 600 | 246 | 17100 | 0.668 | 299 | 2 | 105 | 80.6 | 10566 | 10566 | 4642 | 4.62 | 4.62 |
| Liu et al. [19] | S43[c] | 260 | 780 | 246 | 17100 | 0.334 | 299 | 2 | 105 | 80.6 | 2325 | 7101 | 6567 | 2.73 | 3.98 |
| Liu et al. [19] | S44[c] | 260 | 780 | 246 | 17100 | 0.334 | 299 | 2 | 105 | 80.6 | 3174 | 7453 | 6568 | 2.65 | 3.98 |
| Liu et al. [19] | S45[c] | 260 | 780 | 246 | 17100 | 0.334 | 299 | 2 | 105 | 80.6 | 2018 | 7161 | 6514 | 2.69 | 4.07 |

| | | | | | | | | | | | | | | | |
|---|---|---|---|---|---|---|---|---|---|---|---|---|---|---|---|
| Liu et al. [19] | S46[c] | 260 | 780 | 246 | 17100 | 0.668 | 299 | 2 | 105 | 80.6 | 2687 | 5778 | 6269 | 2.43 | 4.00 |
| Liu et al. [19] | S47[c] | 260 | 780 | 246 | 17100 | 0.668 | 299 | 2 | 105 | 80.6 | 2685 | 6401 | 6332 | 2.66 | 4.92 |
| Liu et al. [19] | S48[c] | 260 | 780 | 246 | 17100 | 0.668 | 299 | 2 | 105 | 80.6 | 2093 | 9408 | 6374 | 2.77 | 4.64 |
| Liu et al. [19] | S49[b] | 260 | 780 | 246 | 17100 | 0.835 | 299 | 2 | 105 | 80.6 | 4891 | 8377 | 6927 | 2.52 | 5.18 |
| Ran [20] | S50[b] | 172 | 510 | 245 | 15100 | 0.167 | 188 | 1 | 68.7 | 54.7 | 1750 | 8200 | 1787 | 2.39 | 5.508 |
| Ran [20] | S51[a] | 172 | 510 | 245 | 15100 | 0.334 | 188 | 1 | 68.7 | 54.7 | 6300 | 6300 | 2289 | 7.395 | 7.395 |
| Ran [20] | S52[a] | 172 | 510 | 245 | 15100 | 0.501 | 188 | 1 | 68.7 | 54.7 | 5200 | 5200 | 2574 | 6.783 | 6.783 |
| Ran [20] | S53[c] | 174 | 510 | 245 | 15100 | 0.167 | 192 | 2 | 68.7 | 54.7 | 2280 | 6800 | 2090 | 2.35 | 7.45 |
| Ran [20] | S54[a] | 174 | 510 | 245 | 15100 | 0.334 | 192 | 2 | 68.7 | 54.7 | 7000 | 7000 | 2602 | 8.874 | 8.874 |
| Ran [20] | S55[a] | 174 | 510 | 245 | 15100 | 0.501 | 192 | 2 | 68.7 | 54.7 | 7400 | 7400 | 3076 | 10.71 | 10.71 |
| Ran [20] | S56[c] | 174 | 510 | 245 | 15100 | 0.334 | 192 | 2 | 81.1 | 63.4 | 1345 | 6300 | 2846 | 2.30 | 6.07 |
| Ran [20] | S57[a] | 174 | 510 | 245 | 15100 | 0.501 | 192 | 2 | 81.1 | 63.4 | 7000 | 7000 | 3316 | 5.41 | 5.41 |
| Ran [20] | S58[c] | 172 | 510 | 80 | 18000 | 0.23 | 188 | 1 | 68.7 | 54.7 | 1310 | 6900 | 1767 | 2.19 | 5.00 |
| Ran [20] | S59[c] | 172 | 510 | 80 | 18000 | 0.46 | 188 | 1 | 68.7 | 54.7 | 2540 | 6900 | 1714 | 2.96 | 7.29 |
| Ran [20] | S60[c] | 174 | 510 | 80 | 18000 | 0.23 | 192 | 2 | 68.7 | 54.7 | 1970 | 8300 | 1921 | 2.70 | 7.75 |
| Ran [20] | S61[b] | 174 | 510 | 80 | 18000 | 0.46 | 192 | 2 | 68.7 | 54.7 | 9900 | 9900 | 2182 | 3.42 | 8.31 |

[a] Specimens with bi-linear type of axial load-strain curves;

[b] Specimens with elastic-plastic type of axial load-strain curves;

[c] Specimens with linear-nonlinear type of axial load-strain curves.

## 2.2 Classification of axial load-strain curves

The typical axial load-strain curves of F-STC columns are shown in Fig. 1, in which the nominal axial strain are calculated by Eq. (2). The load-strain curves experience three stages: initial elastic stage (Stage I), plastic stage (Stage II), and strengthening or softening stage (Stage III). At the initial elastic stage, the axial load increases linearly with axial strain. Then axial strain begins to speed up as the plastic deformation of concrete increases and the curves display variations at the third stage (strengthening or softening stage).

$$\varepsilon_c=\delta/l \tag{2}$$

where $\delta$ and $l$ are the measured axial deformation and gauge length of a specimen, respectively.

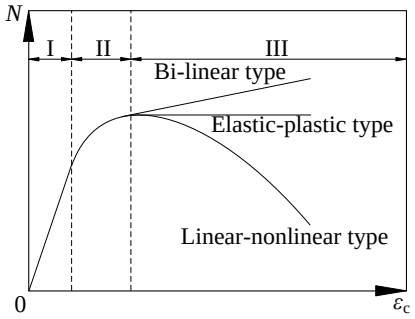


Fig. 1 Typical axial load-strain curves of F-STC columns

The axial load-strain curves of F-STC columns can be divided into three types: bi-linear, elastic-plastic, and linear-nonlinear/parabolic types, as shown in Fig. 1. It is more likely to be bi-linear type when there are more layers of FRP, lower concrete strength, and smaller $D/t_s$, therefore, the confinement ratio ($f_l/f_{co}$) is adopted to classify the axial load-strain curves [19], where $f_l$ is the confining stress at ultimate condition and can be determined by Eqs. (25)-(27) in Section 3.3. As shown in Fig. 2, the bi-linear type is more likely when $f_l/f_{co}>0.2$, or the linear-nonlinear type is the more likely type. Note that the critical value of 0.2 is determined to ensure a relatively conservative prediction as some specimens with bi-linear type of axial load-strain curves are classified into linear-non-linear type. It is obvious that all curves have two important conditions: the peak load condition and the ultimate condition. The peak load condition means that the load reaches the load bearing capacity of columns, while the ultimate condition is defined as the time when the rupture of FRP jackets occurs. For F-STC columns with bi-linear type of load-strain curves, the peak condition can also be treated as ultimate condition as FRP ruptures at peak load, while for F-STC columns with elastic-plastic or linear-parabolic type of load-strain curves, these two conditions are totally different as rupture of FRP occurs beyond peak load.

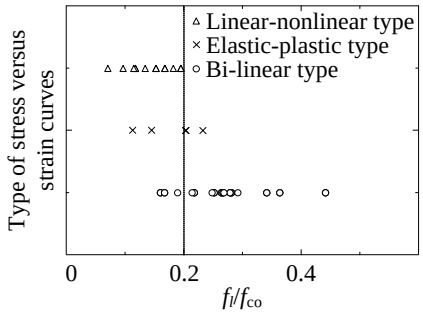


Fig. 2 Type of load-axial shortening curve versus confinement ratio

## 3 Confining stress

## 3.1 Stresses of steel tube at peak load

The axial stress of steel tube in F-STC columns mainly accumulates from the frictional stress between steel tube and concrete as the steel tube does not bear any direct axial load. Therefore, the steel tube only bears transverse stress at the disconnected section, while it is in plane stress state at the middle section. Referring to the methods adopted by Wang [40], equations of the stress distribution of steel tube are established, which are based on the following assumptions.

(1) Deformation of core concrete distributes evenly along the height, which means that the axial and transverse strains of concrete maintain constant at different section.

(2) The transverse strains of FRP, steel tube, and concrete equal to each other.

(3) Slip between steel tube and concrete will not disappear until the axial strain of steel tube accumulates to be equal to that of concrete during the loading process. The frictional coefficient $\mu$ is taken as 0.3 for a flat thin-walled steel tube [41-42].

(4) The steel tube yields along the height at the peak load.

(5) The axial stress of FRP is neglected.

As shown in Fig. 3, a coordinate system is established from the disconnected section. The steel tube cell is subjected to the axial stress and frictional stress ($f$) in the axial direction, in which the frictional stress is induced by the outward confining stress at peak load ($f_{l,\mathrm{p}}$).

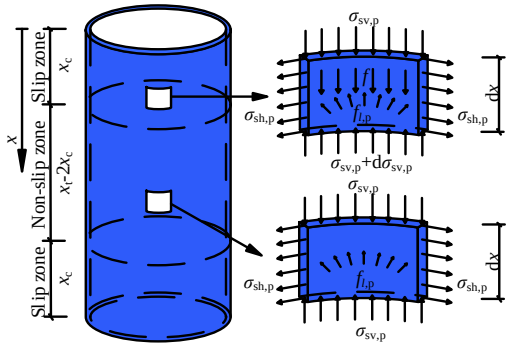


Fig. 3 Stress distribution of steel tube at peak load

Force equilibrium equations in the axial direction are established for the d$x$ height steel tube cell, in which $\sigma_{\mathrm{sv,p}}$, $\sigma_{\mathrm{sh,p}}$ , $f_{ls,\mathrm{p}}$, $f_{lf,\mathrm{p}}$ are the longitudinal and transverse stress of steel tube at peak load, and confining stress provided by steel tube and FRP, respectively.

$$\sigma_{\mathrm{sv,p}}\pi Dt_{\mathrm{s}}+f\pi D\mathrm{d}x=(\sigma_{\mathrm{sv,p}}+\mathrm{d}\sigma_{\mathrm{sv,p}})\pi Dt_{\mathrm{s}} \tag{3}$$

$$f=\mu f_{l,\mathrm{p}}=\mu(f_{ls,\mathrm{p}}+f_{lf,\mathrm{p}}) \tag{4}$$

$$f_{ls,\mathrm{p}}=2t_{\mathrm{s}}\sigma_{\mathrm{sh,p}}/D \tag{5}$$

$$f_{lf,\mathrm{p}}=2t_{\mathrm{f}}\sigma_{\mathrm{f\theta,p}}/D \tag{6}$$

And $\sigma_{\mathrm{f\theta,p}}$ is the transverse stress of FRP at peak load , which can be determined by Eq. (7).

$$\sigma_{\mathrm{f\theta,p}}=E_{\mathrm{frp}}\varepsilon_{\mathrm{fp}} \tag{7}$$

Plugging Eqs. (4)-(6) into Eq. (3), the following equation can be obtained.

$$\sigma_{\mathrm{sh,p}}=\frac{D}{2\mu}\frac{\mathrm{d}\sigma_{\mathrm{sv,p}}}{\mathrm{d}x}-\frac{t_{\mathrm{f}}}{t_{\mathrm{s}}}\sigma_{\mathrm{f\theta,p}} \tag{8}$$

According to assumption (4), the steel tube yields along the height of the columns, therefore, longitudinal and transverse stress of steel tube meet the von Mises yield criterion.

$$\sigma_{\mathrm{sv,p}}^2+\sigma_{\mathrm{sh,p}}^2-\sigma_{\mathrm{sv,p}}\sigma_{\mathrm{sh,p}}=f_{\mathrm{y}}^2 \tag{9}$$

Then, Eq. (10) is obtained.

$$\left(\frac{D}{\mu}\frac{\mathrm{d}\sigma_{\mathrm{sv,p}}}{\mathrm{d}x}-\frac{2t_{\mathrm{f}}}{t_{\mathrm{s}}}\sigma_{\mathrm{f\theta,p}}-\sigma_{\mathrm{sv,p}}\right)^{2}+\left(\sqrt{3}\sigma_{\mathrm{sv,p}}\right)^{2}=\left(2f_{\mathrm{y}}\right)^{2} \tag{10}$$

To solve the function, parameter $\theta$ is introduced. Therefore, Eq. (10) can be rewritten as Eqs. (11) and (12).

$$\frac{D}{\mu}\frac{\mathrm{d}\sigma_{\mathrm{sv,p}}}{\mathrm{d}x}-\frac{2t_{\mathrm{f}}}{t_{\mathrm{s}}}\sigma_{\mathrm{f\theta,p}}-\sigma_{\mathrm{sv,p}}=2f_{\mathrm{y}}\cos\theta \tag{11}$$

$$\sqrt{3}\sigma_{\mathrm{sv,p}}=-2f_{\mathrm{y}}\sin\theta \tag{12}$$

where $\sigma_{\mathrm{sv,p}}\in[-f_{\mathrm{y}},0]$, and $\theta\in[0,\pi/3]$. Solve Eqs. (11) and (12), and the following result is obtained.

$$\frac{\mathrm{d}x}{\mathrm{d}\theta}=\frac{D\cos\theta}{\mu\left(\sin\theta-\sqrt{3}\cos\theta-a\right)} \tag{13}$$

where $a=\frac{\sqrt{3}t_{\mathrm{f}}\sigma_{\mathrm{f\theta,p}}}{t_{\mathrm{s}}f_{\mathrm{y}}}$, and Eq. (14) is then obtained after integration.

$$x=\begin{cases}\dfrac{D}{4\mu}\ln\left|\sin\left(\theta-\dfrac{\pi}{3}\right)-a\right|-\dfrac{\sqrt{3}D}{4\mu}\theta-\dfrac{\sqrt{3}aD}{2\mu\sqrt{a^2-1}}\tan^{-1}\left(\dfrac{1-a\tan\left(\frac{\theta}{2}-\frac{\pi}{6}\right)}{\sqrt{a^2-1}}\right)+\mathrm{C}_1 & a\geq 1\\ \dfrac{D}{4\mu}\ln\left|\sin\left(\theta-\dfrac{\pi}{3}\right)-a\right|-\dfrac{\sqrt{3}D}{4\mu}\theta-\dfrac{\sqrt{3}aD}{4\mu\sqrt{1-a^2}}\ln\left|\dfrac{a\tan\left(\frac{\theta}{2}-\frac{\pi}{6}\right)+\sqrt{1-a^2}-1}{a\tan\left(\frac{\theta}{2}-\frac{\pi}{6}\right)-\sqrt{1-a^2}-1}\right|+\mathrm{C}_2 & a<1\end{cases} \tag{14}$$

To obtain the value of constants C1 and C2, boundary condition is plugged here, which means $x$=0 when $\theta$=0.

$$\mathrm{C}_1=\frac{\sqrt{3}aD}{2\mu\sqrt{a^2-1}}\tan^{-1}\left(\frac{\sqrt{3}a+3}{3\sqrt{a^2-1}}\right)-\frac{D}{4\mu}\ln\left(\frac{\sqrt{3}}{2}+a\right) \tag{15}$$

$$\mathrm{C}_2=\frac{\sqrt{3}aD}{4\mu\sqrt{1-a^2}}\ln\left|\frac{\sqrt{3}a+\sqrt{1-a^2}-1}{\sqrt{3}a-\sqrt{1-a^2}-1}\right|-\frac{D}{4\mu}\ln\left(\frac{\sqrt{3}}{2}+a\right) \tag{16}$$

The parametric stress distribution equations of steel tube along the height of column ($x$) are shown below.

$$\sigma_{\mathrm{sv,p}}=-\frac{2\sqrt{3}}{3}\sin(\theta)f_{\mathrm{y}} \tag{17}$$

$$\sigma_{\mathrm{sh,p}}=-\frac{\sqrt{3}f_{\mathrm{y}}}{3}\left(\sin\theta-\sqrt{3}\cos\theta-a\right)-\frac{t_{\mathrm{f}}}{t_{\mathrm{s}}}\sigma_{\mathrm{f\theta,p}} \tag{18}$$

$$\frac{x}{D}=\begin{cases}\dfrac{\ln\left|\sin\left(\theta-\dfrac{\pi}{3}\right)-a\right|-\sqrt{3}\theta-\dfrac{2\sqrt{3}a}{\sqrt{a^2-1}}\tan^{-1}\left(\dfrac{1-a\tan\left(\frac{\theta}{2}-\frac{\pi}{6}\right)}{\sqrt{a^2-1}}\right)}{4\mu}+\dfrac{\mathrm{C}_1}{D} & \mathrm{a}\geq 1\\ \dfrac{\ln\left|\sin\left(\theta-\dfrac{\pi}{3}\right)-a\right|-\sqrt{3}\theta-\dfrac{\sqrt{3}a}{\sqrt{1-a^2}}\ln\left|\dfrac{a\tan\left(\frac{\theta}{2}-\frac{\pi}{6}\right)+\sqrt{1-a^2}-1}{a\tan\left(\frac{\theta}{2}-\frac{\pi}{6}\right)-\sqrt{1-a^2}-1}\right|}{4\mu}+\dfrac{\mathrm{C}_2}{D} & \mathrm{a}<1\end{cases} \tag{19}$$

As shown in Fig. 4, the transverse stress of steel tube decreases from $f_{\mathrm{y}}$ at the disconnected section to a certain value at a middle section, while the longitudinal stress accumulates from 0 at the disconnected section to a certain value at a middle section, both are highly related to the location of

steel tube. But it should be noted that all equations are established based on the assumption (3), indicating that the results are unavailable at sections where there is no slip between concrete and steel tube. After the height of column exceeds the critical section $x_c$, the stresses of steel tube maintain stable, therefore, it is very crucial to determine the critical section.

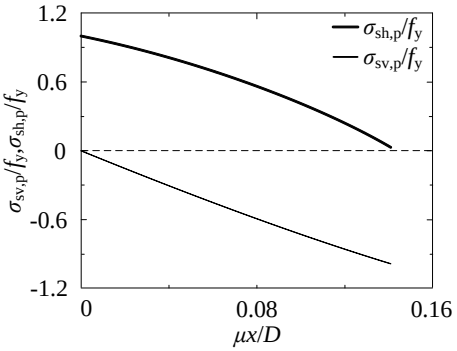


Fig. 4 Typical tube stresses versus $\mu x/D$ curves

The values of $\mu x_c/D$ are solved based on existing test results, as shown in Fig. 5. Most of the values of $\mu x_c/D$ are in the range of 0-0.2 with a mean value of 0.073 and standard deviation of 0.034. Therefore, the height of the critical section is $x_c=0.073D/\mu=0.24D$. As shown in Fig. 4, it is obvious that the stresses of steel tube distribute approximately linearly between the disconnected section and critical section.

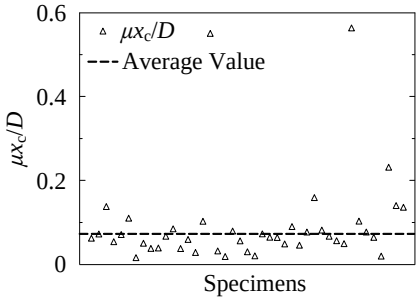


Fig. 5 Statistic results of $\mu x_c/D$ in the tests

Therefore, expressions of stress distribution of steel tube at peak load are obtained, as shown in Eqs. (20) and (21).

$$\frac{\sigma_{sv,p}}{f_y}=\begin{cases}-7.26\mu\dfrac{x}{D} & 0\le x<x_c\\ -0.53 & x\ge x_c\end{cases} \tag{20}$$

$$\frac{\sigma_{sh,p}}{f_y}=\begin{cases}1-5.2\mu\dfrac{x}{D} & 0\le x<x_c\\ 0.62 & x\ge x_c\end{cases} \tag{21}$$

Based on Eqs. (20) and (21), the stress distribution of steel tube can be illustrated, as shown in Fig. 6.

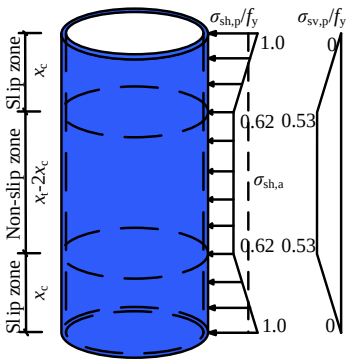


Fig. 6 Typical stress distribution of steel tube of F-STC columns at peak load

Equivalent transverse stress ($\sigma_{sh,a}$) is adopted to reflect the average confinement provided by steel tube, as shown in Eqs. (22) and (23), in which $K_{hf}$ is the equivalent transverse stress factor and $x_t$ is the length of the continuous steel tube. It should be noted that the stresses of steel tube keep constant in the non-slip zone and the length of slip zone is relatively small, therefore, it is reasonable to adopt the same calculation methods for the stress of steel tube at ultimate condition for F-STC columns with elastic-plastic or linear-parabolic stress-strain curves.

$$\sigma_{sh,a}=K_{hf}f_y \tag{22}$$

$$K_{hf}=\begin{cases}1\text{-}0.39\dfrac{x_t}{D} & x_t<0.48D\\ 0.62+0.09\dfrac{D}{x_t} & x_t\geq 0.48D\end{cases} \tag{23}$$

## 3.2 Strain of FRP at peak load

It is very interesting that the rupture strain of FRP is smaller than that obtained from flat coupon test, which is demonstrated in previous studies [17, 23, 26, 43]. And this phenomenon is probably caused by the following several reasons [44-47].

(1) Curvature of FRP sheets. The FRP coupons are fabricated to be flat for material mechanical test, while FRP jackets are wrapped around the columns in practical application.

(2) Multi-directional stress state. Uniaxial tensile force is applied to FRP coupons, while it is also subjected to longitudinal and lateral stresses.

(3) Geometric deficiency of steel tube. This will lead to the uneven deformation of FRP.

(4) Overlapping zone of FRP jackets. Test results indicate that the transverse strain of FRP in overlapping zone is smaller than that out of overlapping zone.

(5) Inhomogeneity of concrete. Cracks of concrete develop randomly, which will lead to stress concentration in FRP jackets.

To determine the confining stress of FRP, it is very important to predict the rupture strain of FRP. Strain efficiency factor $K_\varepsilon$ is adopted to account for the difference of rupture strains between the test results and flat coupon tests [43, 46]. Based on the regression analysis on the measured strain efficiency factor, an empirical model adopted the similar form proposed by Lim and Ozbakkaloglu [48] for predicting the rupture strain of FRP is obtained and shown in Eq. (24).

$$K_\varepsilon=0.7\text{-}2.87\times10^{-5}\frac{E_{frp}t_f}{D}\text{-}0.0012f_{co} \tag{24}$$

It should be noted that for specimens with elastic-plastic or linear-parabolic type stress-strain curves, FRP generally ruptures beyond the peak load (Table 1). The ratio between the transverse strain at

the peak load and rupture strain given by the manufacturer of these two types of specimens ($K_{\varepsilon p}$) is shown in Fig. 7, and the mean value is approximately 0.134. Note that for some specimens with elastic-plastic type axial load-strain curves, the horizontal branch maybe fluctuating, leading to an overestimation of FRP rupture strain at peak load condition. Thus these data are excluded for the prediction of $K_{\varepsilon p}$.

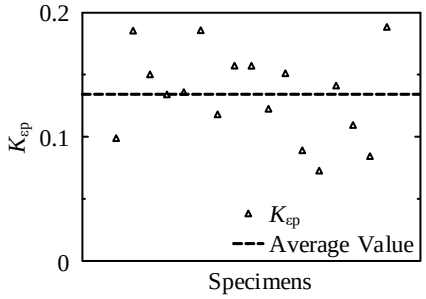


Fig. 7 Strain efficiency factor of FRP at peak load for FRP-steel composite tubed concrete columns with elastic-plastic or linear-parabolic stress-strain curves

## 3.3 Confining stress

The confining stress of FRP-steel composite tubed concrete columns at ultimate condition ($f_l$) consists of confining stress provided by FRP ($f_{lf}$) and steel tube ($f_{ls}$). And the confining stress at peak load ($f_{l,p}$) is calculated by replacing the strain efficiency factor $K_\varepsilon$ with $K_{\varepsilon p}$. It should be noted that the transverse strains of FRP and steel are essentially the same, which is indeed an important assumption in the determination of tube stress (Assumption (2), Section 3.1). However, this assumption is not explicitly reflected in Eqs. (26) and (27), but is implicitly used in developing the equations (Eq. (23)) for $K_{hf}$, which is an important factor in Eq. (26) for calculating the confining pressure provided by the steel tube.

$$f_l = f_{ls} + f_{lf} \tag{25}$$

$$f_{ls} = \frac{2K_{hf}t_s f_y}{D} \tag{26}$$

$$f_{lf} = \frac{2K_\varepsilon \varepsilon_{fu} E_{frp} t_f}{D} \tag{27}$$

# 4 Design-oriented model

## 4.1 Peak condition of F-STC columns

### 4.1.1 Axial load bearing capacity

Four existing models were selected to be verified with the load bearing capacity of F-STC columns. In this study, a new model is proposed with the same form as Richart et al.'s model ($f_{cc}/f_{co}=1+Kf_l/f_{co}$) [53] and the confinement effectiveness coefficient $K$ is valued as 3.26 based on the regression analysis of test results. Details of calculated models are shown in Table 2. To simplify the calculation methods for the load bearing capacity of F-STC columns with different types of stress-strain curves, the proposed model is applicable to all kinds of F-STC columns. This is realized by using rupture strain rather than the transverse strain at peak load to calculate the confining stress of F-STC columns with elastic-plastic or linear-nonlinear types of axial load-strain curves, which is reasonable

considering the following two facts.

(1) For F-STC columns with elastic-plastic or linear-nonlinear types of stress-strain curves, the transverse strain of FRP at peak load is much lower than rupture strain, providing approximately 20% of the maximum lateral confining stress of FRP. The confinement ratio is small ($\frac{f_l}{f_{co}}$<0.1), therefore, the coefficient $K$ needs to be large enough to accurately predict the axial bearing capacity.

(2) For F-STC specimens with bi-linear type stress-strain curves, rupture strain is used to calculate lateral confining stress. Therefore, the coefficient $K$ is valued as 3.26, which is smaller than that of F-STC columns with elastic-plastic or linear-parabolic stress-strain curves.

Therefore, using rupture strain to calculate confining stress is an alternative to increase the coefficient $K$, resulting in a unified model for the calculation of load bearing capacity.

Table 2 Models for load bearing capacity

| Reference | Details of models | |
|---|---|---|
| Mander[49] | $f_{fc}=f_{co}\left(-1.254+2.254\sqrt{1+7.94\frac{f_l}{f_{co}}}-2\frac{f_l}{f_{co}}\right)$ | (28) |
| Li[50] | $f_{fc}=f_{co}\left(-0.413+1.413\sqrt{1+11.4\frac{f_l}{f_{co}}}-2\frac{f_l}{f_{co}}\right)$ | (29) |
| Xiao[51] | $f_{fc}=f_{co}\left(1+3.24\left(\frac{f_l}{f_{co}}\right)^{0.8}\right)$ | (30) |
| Teng[52] | $f_{fc}=f_{co}\left(1+3.5\frac{f_l}{f_{co}}\right)$ | (31) |
| Proposed model | $f_{fc}=f_{co}\left(1+3.26\frac{f_l}{f_{co}}\right)$ | (32) |

The load bearing capacity can be determined by Eq. (33), in which the cross section area is taken as gross area and the axial stress of steel tube is neglected. This is mainly because of the following two reasons: (1) the $D/t_s$ is relatively large, resulting in relatively small area of steel tube; (2) the steel tube in F-STC does not bear any direct axial load. Therefore, the contribution of axial stress of steel tube to the load bearing capacity of F-STC columns is limited. In addition, a parametric study has been conducted on the comparison of two kinds of calculation methods for the load bearing capacity of F-STC columns: one employs Eq. (33) to calculate the load bearing capacity, the other considers the axial stress of steel tube and concrete, respectively. The difference between these two methods is within 10%, which indicates that the neglect of axial stress of steel tube is reasonable.

$$N_p^c=f_{fc}A \tag{33}$$

Fig. 8 shows the comparison between the predicted results ($N_p^c$) and experimental results ($N_p^e$), in which X and S are the average value and standard deviation of the ratio between the calculation results and experimental results. As shown in Fig. 8, Mander's and Xiao's models overestimate the load bearing capacity, while Li's model underestimates the test results. Teng's model coincides better with the test results and the proposed model agrees best with the experimental results among the five models.

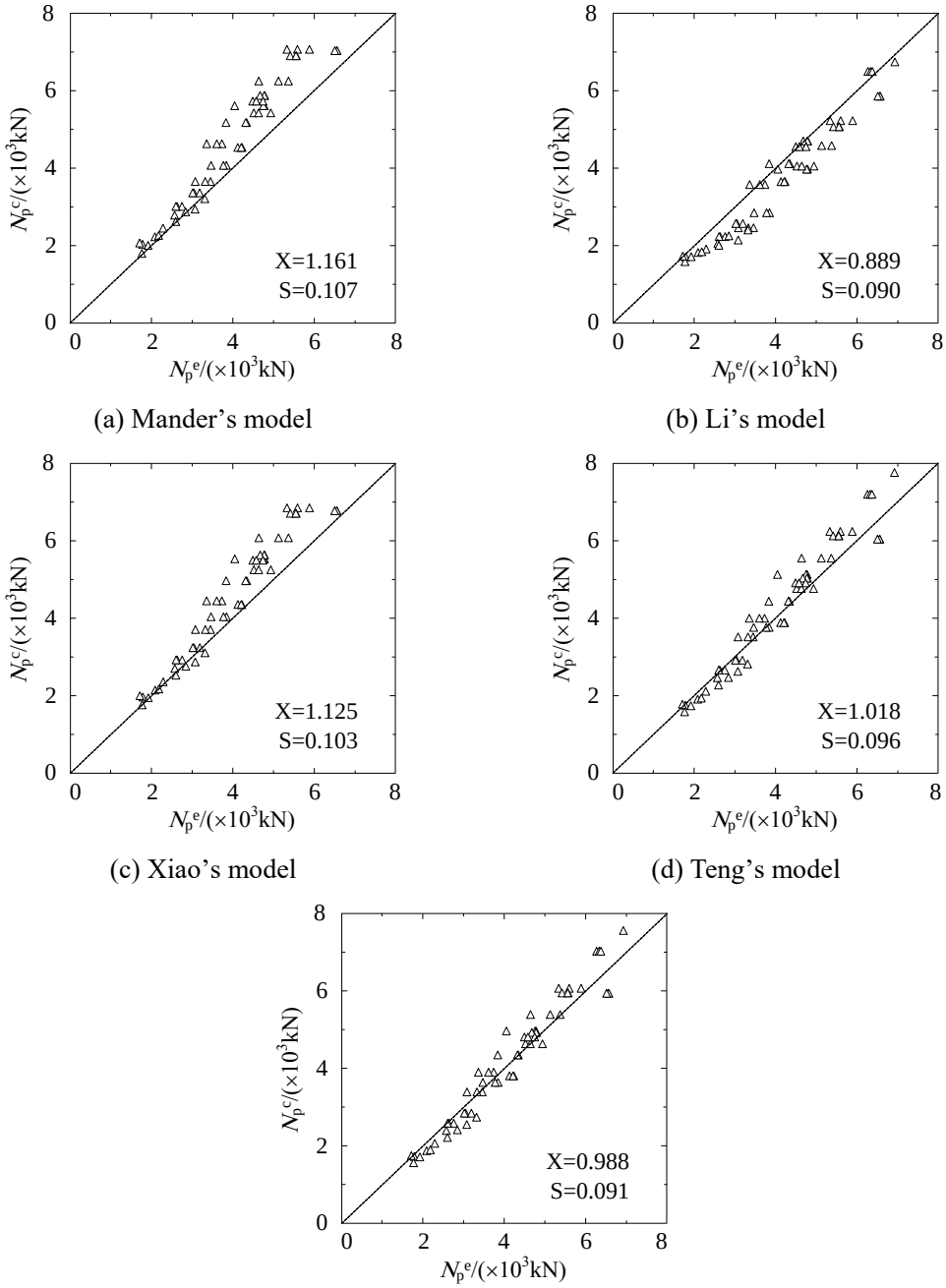


(a) Mander's model (b) Li's model

(c) Xiao's model (d) Teng's model

(e) Proposed model

Fig. 8 Verification of calculation results

## 4.1.2 Axial strain at peak load

As shown in Table 3, three existing models and one proposed model for predicting the axial strain at peak load were used to be verified with the test results, in which the confining stress is calculated by Eqs. (25)-(27).

Table 3 Models for peak axial strain

| Reference | Details of models |
|---|---|
| Mander[49] | $\varepsilon_{fc}^c=\varepsilon_{co}\left(1+5\left(\frac{f_{fc}}{f_{co}}-1\right)\right)$ (34) |

| | | |
|---|---|---|
| Teng[52] | $\varepsilon_{\mathrm{fc}}^{\mathrm{c}}=\varepsilon_{\mathrm{co}}\left(1+17.5\left(\frac{f_{\mathrm{l}}}{f_{\mathrm{co}}}\right)^{1.2}\right)$ | (35) |
| Attard[54] | $\varepsilon_{\mathrm{fc}}^{\mathrm{c}}=\varepsilon_{\mathrm{co}}\left(1+\left(17\text{-}0.06f_{\mathrm{co}}\right)\frac{f_l}{f_{\mathrm{co}}}\right)$ | (36) |
| Proposed model | $\varepsilon_{\mathrm{fc}}^{\mathrm{c}}=\begin{cases}\varepsilon_{\mathrm{co}}\left(1+\left(27\text{-}0.12f_{\mathrm{co}}\right)\frac{f_l}{f_{\mathrm{co}}}\right) & \frac{f_l}{f_{\mathrm{co}}}>0.2\\ \varepsilon_{\mathrm{co}}\left(1+\left(38\text{-}0.31f_{\mathrm{co}}\right)\frac{f_{l,\mathrm{p}}}{f_{\mathrm{co}}}\right) & \frac{f_l}{f_{\mathrm{co}}}\le 0.2\end{cases}$ | (37) |

The comparison between calculation results and test results is shown in Fig. 9. The predicted results of Mander's model, Teng's model and Attard's model underestimate the test results, while the proposed model agrees well with test results.

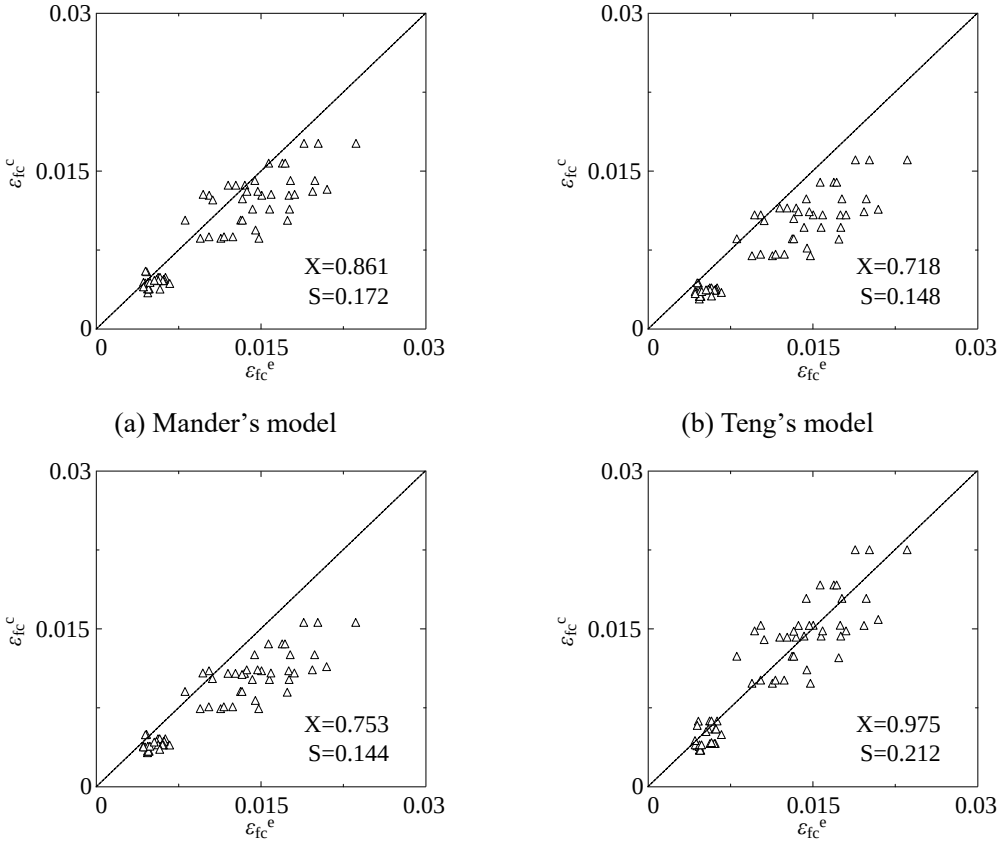


(a) Mander's model (b) Teng's model

(c) Attard's model (d) Proposed model

Fig. 9 Verification of calculation results

## 4.2 Ultimate condition of F-STC columns

As for F-STC columns with elastic-plastic and linear-parabolic types of stress-strain curves, a new model for the calculation of ultimate strain needs to be proposed. Based on the regression analysis on the ultimate strain of these two types of columns, the calculation method for the ultimate strain can be obtained.

$$\varepsilon_{cu}^{c}=\varepsilon_{co}\left(1+\left(49-0.43f_{co}\right)\frac{f_l}{f_{co}}\right) \tag{38}$$

As shown in Fig. 10, the calculated results of the proposed model are generally in good agreement with the test results despite the relatively scatter of the test results. A larger database is needed for the development of an improved model in the future.

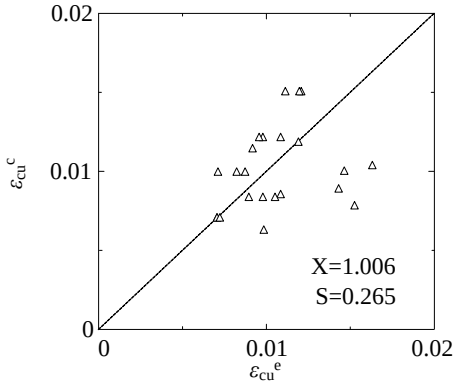


Fig. 10 Verification of calculation results

## 4.3 Peak condition of STC columns

A large database for the circular and square STC columns under axial compression was assembled by Wang [40], which covers a wide range of parameters: concrete strength (34.5MPa-95.2MPa), yield stress of steel tube (185.7MPa-448MPa), diameter/width-to-thickness ratio of steel tube (64-221), and continuous length-to-diameter/width ratio of steel tube (0.6-5.9). In wang's study, the peak load bearing capacity and corresponding axial strain of STC columns are suggested to be predicted by Eqs. (39) and (40).

$$f_{sc}=f_{co}\left(1+5.1\frac{f_{le}}{f_{co}}\right) \tag{39}$$

$$\varepsilon_{sc}=\varepsilon_{co}\left(1+\left(17-0.06f_{co}\right)\frac{f_{le}}{f_{co}}\right) \tag{40}$$

$$f_{le}=\frac{2K_h t_s f_y}{D} \tag{41}$$

$$K_h=-0.1\frac{x_t}{D}+1\geq 0.5 \tag{42}$$

## 4.4 Design formulas

### 4.4.1 Bi-linear type

A lot of design-oriented models have been developed for FRP confined concrete columns, which have been reviewed and assessed by Ozbakkaloglu et al. [55]. And Lam and Teng's model is the most accurate and possesses a relatively simple form [3]. With some modification, this model has been applied to ACI-440.2R [56] and the design guidance issued by the Concrete Society in the UK [57]. The proposed design-oriented model is modified from Teng's model, which is based on the following assumptions.

(1) The nominal stress-strain curve consists of a parabolic branch and a linear branch, as shown in

Fig. 11.

(2) The parabolic branch meets the linear branch smoothly, which means that the value and slope at the meeting point ($\varepsilon_t$) are identical for the two branches.

(3) The initial slope of first parabolic branch equals to the elastic modulus of unconfined concrete, and it can be calculated by $E_c=4730\sqrt{f_{co}}$.

(4) The second linear branch terminates at the point where the peak condition of F-STC columns reaches.

(5) The linear branch intercepts the axial stress axis at a stress level the same as the compressive strength of STC columns.

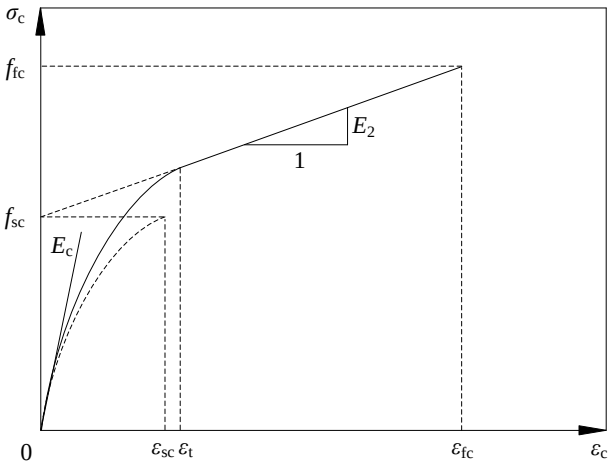


Fig. 11 Design-oriented model for bi-linear F-STC columns

Details of the design-oriented model for bi-linear F-STC columns are described as Eqs. (43)-(45).

$$\sigma_c=\begin{cases} E_c\varepsilon_c-\dfrac{(E_c-E_2)^2}{4f_{sc}}\varepsilon_c^2 & 0\le\varepsilon_c\le\varepsilon_t \\ f_{sc}+E_2\varepsilon_c & \varepsilon_t\le\varepsilon_c\le\varepsilon_{fc} \end{cases} \tag{43}$$

$$E_2=\frac{f_{fc}-f_{sc}}{\varepsilon_{fc}} \tag{44}$$

$$\varepsilon_t=\frac{2f_{sc}}{E_c-E_2} \tag{45}$$

## 4.4.2 Elastic-plastic type

As for F-STC columns with elastic-plastic type of load-strain curves, it is assumed that the design-oriented model is composed of a parabolic branch and a horizontal branch, as shown in Fig. 12.

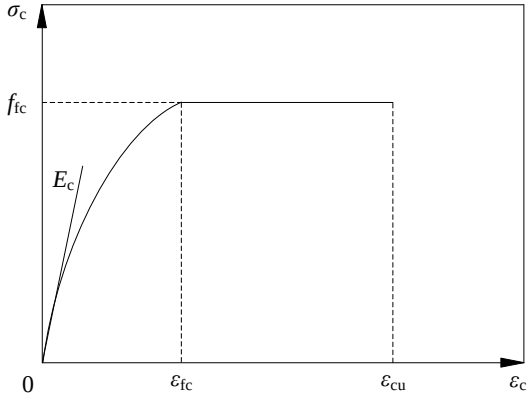

Fig. 12 Design-oriented model for elastic-plastic F-STC columns

The slope of the peak point of parabolic branch equals to zero, details of the proposed model are shown in Eq. (46).

$$\sigma_c=\begin{cases}2\frac{f_{fc}}{\varepsilon_{fc}}\varepsilon_c-\frac{f_{fc}}{\varepsilon_{fc}^2}\varepsilon_c^2 & 0\le\varepsilon_c\le\varepsilon_{fc}\\ f_{fc} & \varepsilon_{fc}\le\varepsilon_c\le\varepsilon_{cu}\end{cases} \tag{46}$$

### 4.4.3 Linear-nonlinear type

Popvics's model is adopted for the design of F-STC columns with linear-nonlinear type of load-strain curves [58]. And a shape correction factor $\sqrt{\frac{f_{co}}{30}}$ is adopted to consider the brittleness of concrete, especially for high-strength concrete [40].

$$\sigma_c=\frac{(\varepsilon_c/\varepsilon_{fc})r}{r-1+(\varepsilon_c/\varepsilon_{fc})^r}f_{fc} \tag{47}$$

$$r=\sqrt{\frac{f_{co}}{30}}\frac{E_c}{E_c-E_{sec}} \tag{48}$$

$$E_{sec}=\frac{f_{fc}}{\varepsilon_{fc}} \tag{49}$$

The axial load is calculated by Eq. (50).

$$N=\sigma_c A \tag{50}$$

A comparison of the design-oriented model with the test results in the database is shown in Fig. 13. As shown in Fig. 2, the type of load-axial shortening curves determined by the classification methods mentioned in Section 2.2 (confinement ratio) may be inconsistent with that obtained from the test results. Therefore, only one predicted curve ("Proposed model") is presented in Fig. 13 if the curve type determined by the classification methods is consistent with that from the test results. When the curve type obtained from the classification methods is inconsistent with that from the test results, two predicted curves are presented in Fig. 13: "Proposed model" and "Proposed model-C". "Proposed model" (solid line) represents the calculated result according to the load-strain curve types obtained from the test results, while "Proposed model-C" (dashed line) denotes the calculated results according to the classification methods. The proposed models are generally in good agreement with the test results.

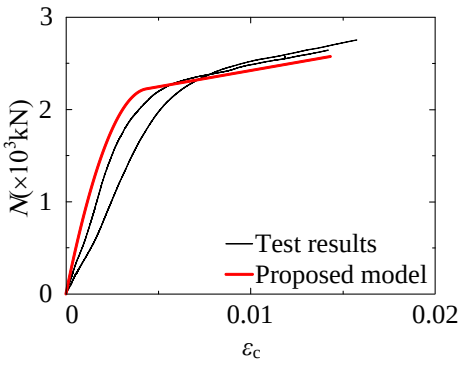


(a) Specimens 1 and 2

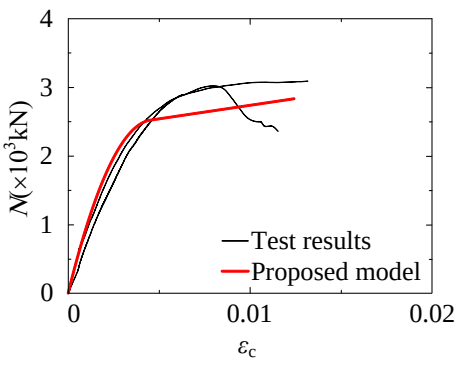


(b) Specimens 3 and 4

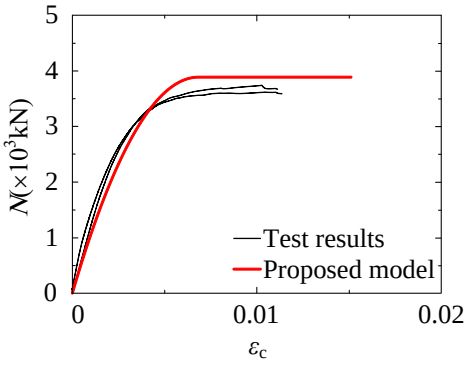


(c) Specimens 5 and 6

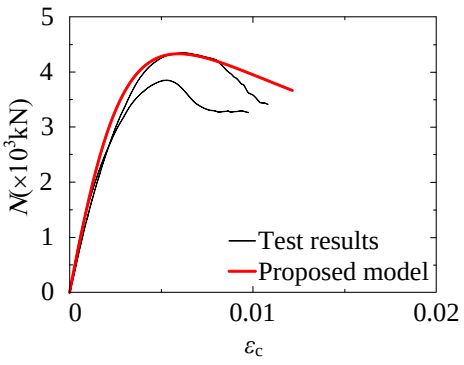


(d) Specimens 7 and 8

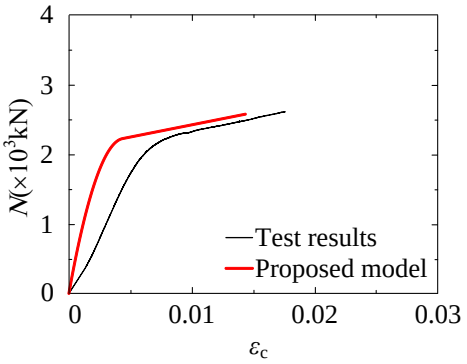


(e) Specimen 9

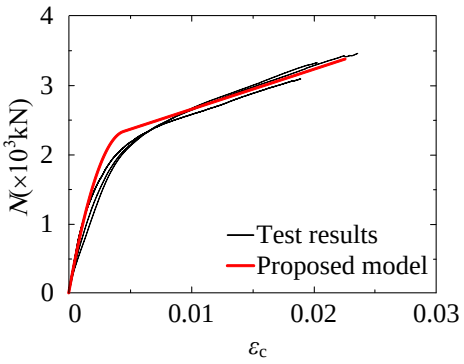


(f) Specimens 10 to 12

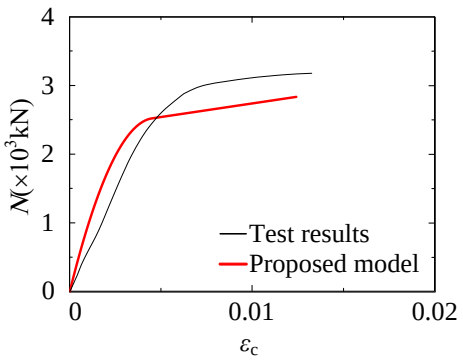


(g) Specimen 13

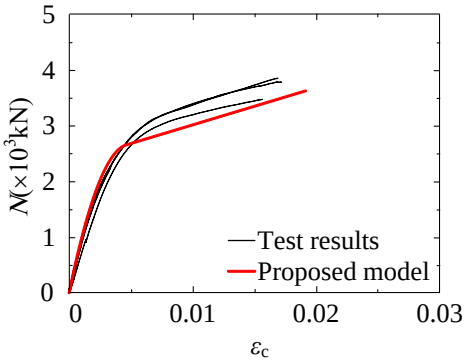


(h) Specimens 14 to 16

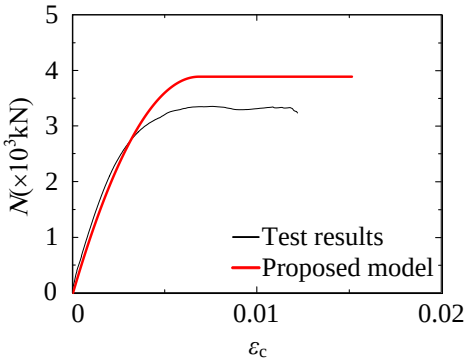


(i) Specimen 17

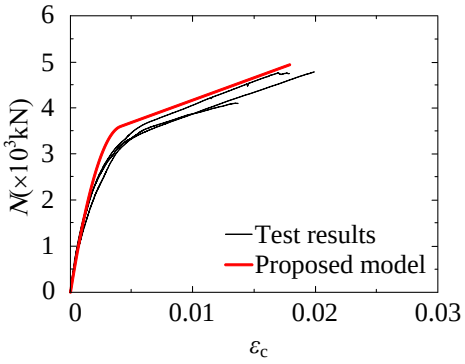


(j) Specimens 18 to 20

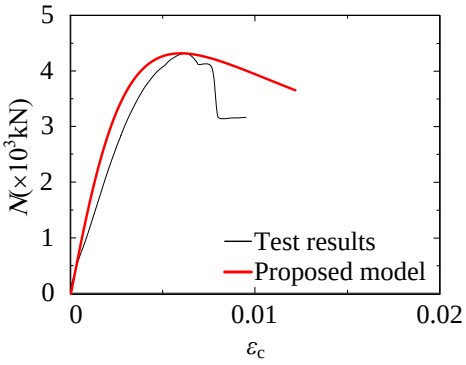


(k) Specimen 21

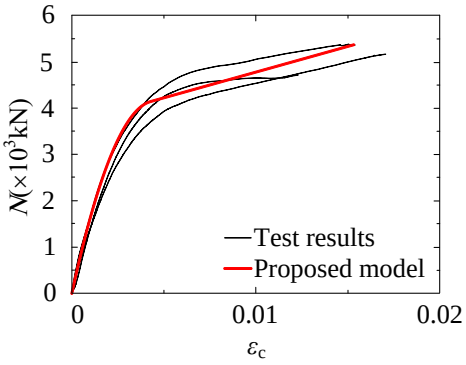


(l) Specimens 22 to 24

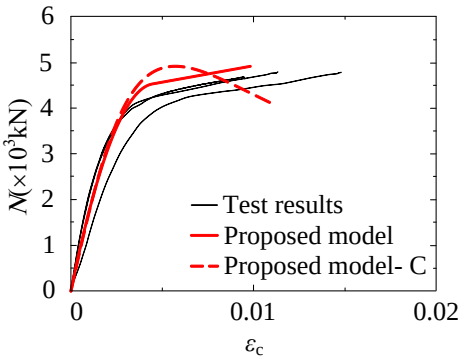


(m) Specimens 25 to 27

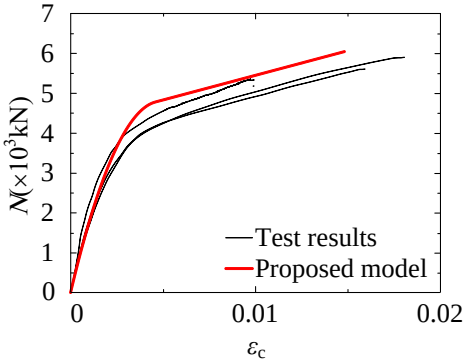


(n) Specimens 28 to 30

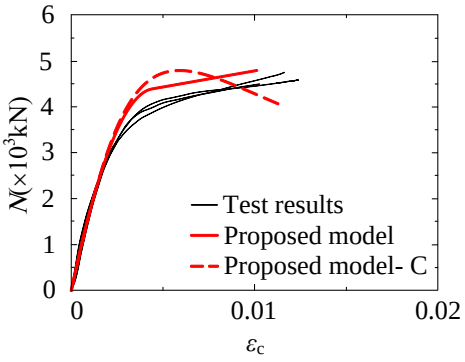


(o) Specimens 31 to 33

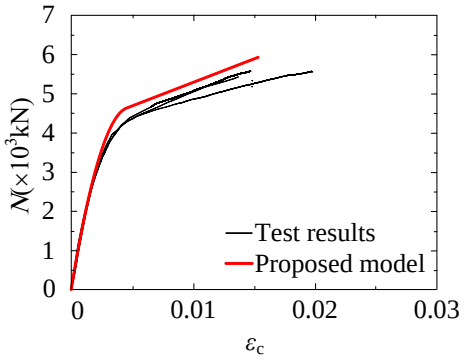


(p) Specimens 34 to 36

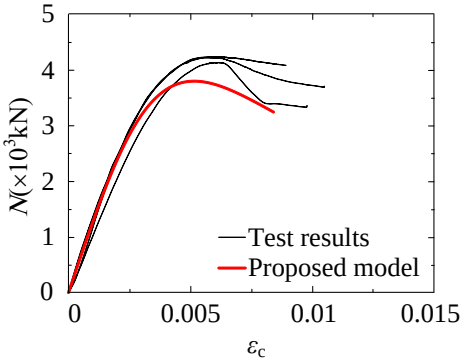


(q) Specimens 37 to 39

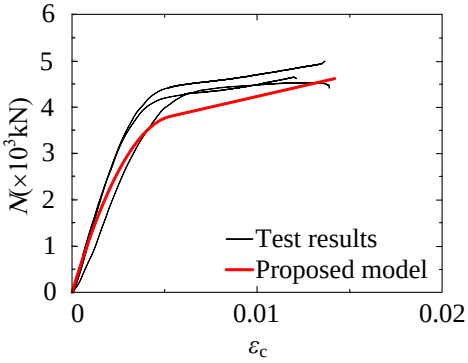


(r) Specimens 40 to 42

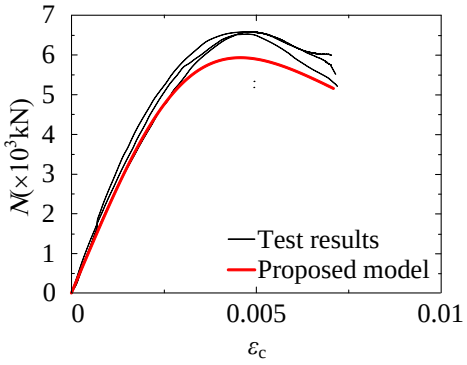


(s) Specimens 43 to 45

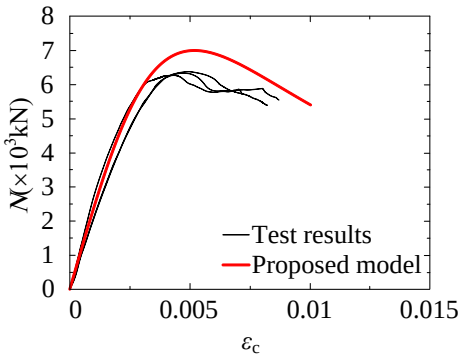


(t) Specimens 46 to 48

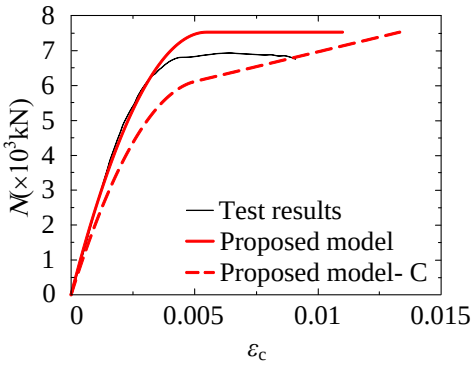


(u) Specimen 49

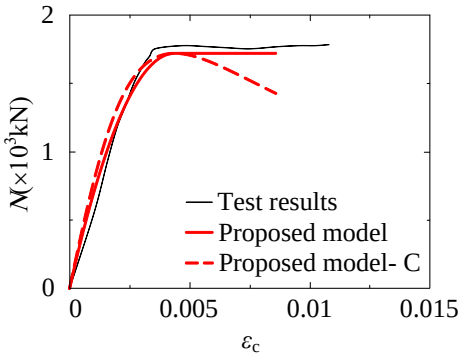


(v) Specimen 50

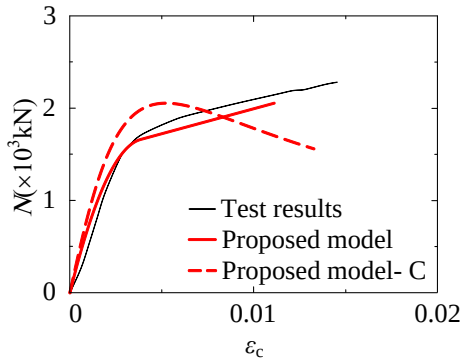


(w) Specimen 51

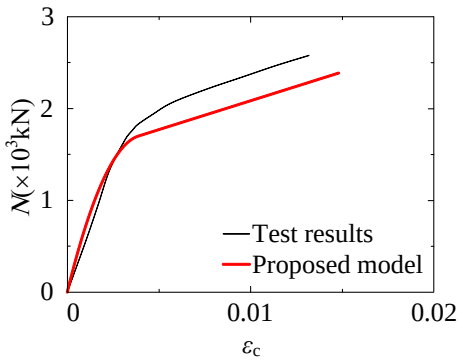


(x) Specimen 52

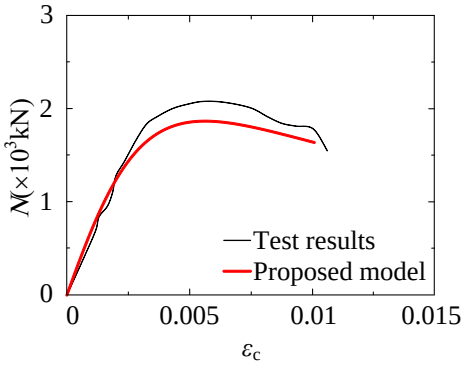


(y) Specimen 53

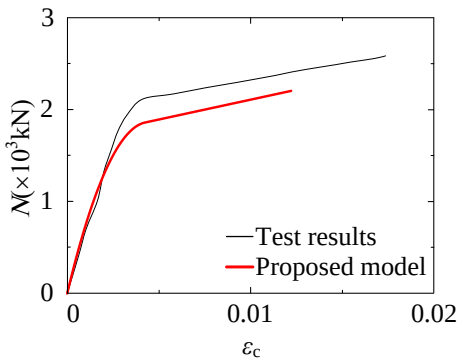


(z) Specimen 54

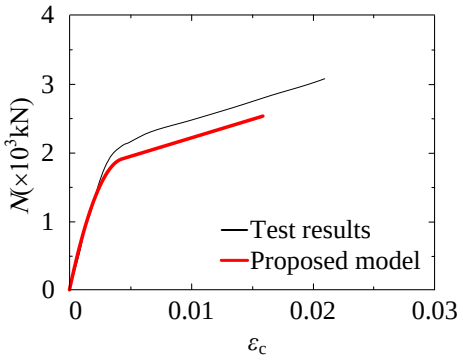


(aa) Specimen 55

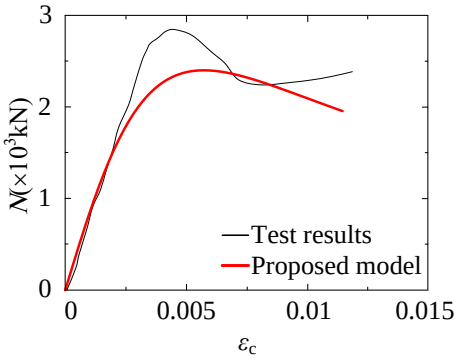


(ab) Specimen 56

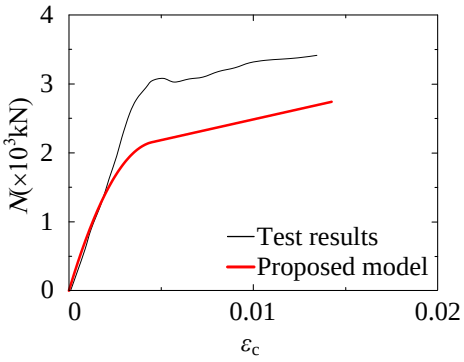


(ac) Specimen 57

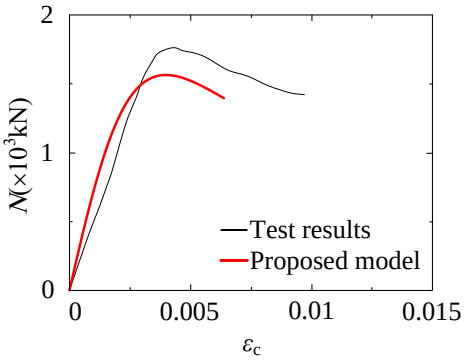


(ad) Specimen 58

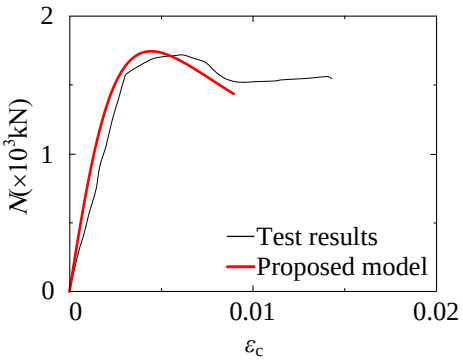


(ae) Specimen 59

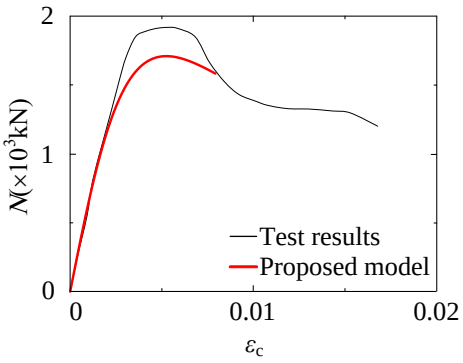


(af) Specimen 60

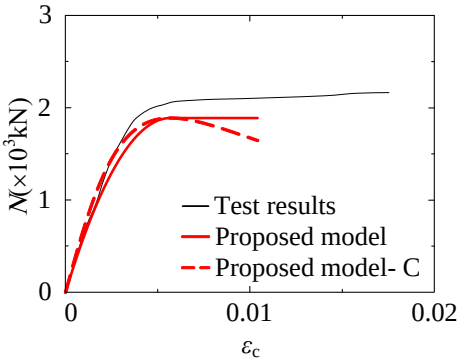


(ag) Specimen 61

Fig. 13 Verification of proposed design-oriented model

# 5 Conclusions

This paper proposed design-oriented models for the axially-loaded FRP-steel composite tubed

concrete stub columns. The proposed models are generated on the basis of a large test database, which are applicable to three different types of F-STC columns. The main conclusions can be summarized as follows.

(1) The axial load-strain curves of F-STC columns can be classified into three types according to the confinement ratio: bi-linear type, elastic-plastic type and linear-nonlinear/parabolic type, and the critical value is 0.2.

(2) The stress distribution of steel tube is analyzed, and equivalent transverse stress is proposed. And an empirical model for the rupture strain of FRP is presented.

(3) Models are selected to be verified with the peak condition of F-STC columns, and new models are proposed for the prediction of load bearing capacity and corresponding axial deformation.

(4) F-STC columns fail by the rupture of FRP, which is defined as the ultimate condition. For F-STC columns with bi-linear load-strain curves, the peak condition is also treated as the ultimate condition, while for F-STC columns with elastic-plastic and linear-parabolic types of load-strain curves, an additional model is proposed to predict the ultimate strain.

(5) Design-oriented models are proposed for these three types F-STC column. As for F-STC columns with bi-linear type of load-strain curves, the design formulas are composed of parabolic and ascending lines, while for elastic-plastic columns, it consists of parabolic-horizontal lines. And a modified Popovics's model is proposed for the design of linear-parabolic columns.

# Notation

| | |
|---|---|
| $a$ | a coefficient related to material properties |
| $A$ | the gross area of a specimen |
| $C_1$ | a constant in the solution of stress distribution functions |
| $C_2$ | a constant in the solution of stress distribution functions |
| $D$ | the diameter of steel tube |
| $\mathrm{d}x$ | the height of the steel tube cell |
| $\mathrm{d}\sigma_{sv,p}$ | the increment of the longitudinal stress of steel tube within $\mathrm{d}x$ |
| $E_2$ | the slope of the linear branch of stress-strain curves of F-STC columns |
| $E_c$ | the elastic modulus of unconfined concrete |
| $E_{frp}$ | the elastic modulus of FRP |
| $E_{sec}$ | the secant modulus of confined concrete |
| $f$ | the frictional stress between steel tube and concrete |
| $f_{co}$ | the unconfined concrete strength |
| $f_{cu}$ | the cubic compressive strength of concrete |
| $f_{fc}$ | the confined concrete strength of F-STC columns |
| $f_l$ | the confining stress of F-STC columns at ultimate condition |
| $f_{le}$ | the confining stress of steel tube in STC columns |
| $f_{l,p}$ | the confining stress of F-STC columns at peak load |
| $f_{lf}$ | the confining stress of FRP at ultimate condition |
| $f_{lf,p}$ | the confining stress of FRP at peak load |
| $f_{ls}$ | the confining stress of steel tube |
| $f_{sc}$ | the confined concrete strength of STC columns |
| $f_y$ | the yield stress of steel tube |
| $K$ | the confinement effectiveness coefficient |

$K_{hf}$ the equivalent transverse stress factor of steel tube in F-STC columns

$K_h$ the equivalent transverse stress factor of steel tube in STC columns

$K_\varepsilon$ the strain efficiency factor of FRP

$K_{\varepsilon p}$ the strain efficiency factor of FRP at peak load for specimens with elastic-plastic and linear-parabolic stress-strain curves

$l$ the gauge length of a specimen

$L$ the length of a specimen

$N$ the axial load of a specimen

$N_p^c$ the calculated bearing capacity of a specimen

$N_p^e$ the measured bearing capacity of a specimen

$t_f$ the thickness of FRP

$t_s$ the thickness of steel tube

$x$ the location of a section at the coordinate system

$x_c$ the location of the critical section at the coordinate system

$x_t$ the length of the continuous steel tube

$\delta$ the measured axial deformation of a specimen

$\delta_p^e$ the measured axial deformation of a specimen at peak load

$\delta_u^e$ the measured axial deformation of a specimen at ultimate condition

$\varepsilon_c$ the axial strain

$\varepsilon_{cu}$ the axial strain of F-STC columns at ultimate condition

$\varepsilon_{fc}^c$ the calculated axial strain of F-STC columns at peak load

$\varepsilon_{fc}^e$ the measured axial strain of F-STC columns at peak load

$\varepsilon_{fp}$ the transverse strain of FRP at peak load

$\varepsilon_{fu}$ the rupture strain of FRP given by manufacturer

$\varepsilon_{rupt}$ the measured rupture strain of FRP

$\varepsilon_{sc}$ the axial strain of STC columns at peak load

$\varepsilon_t$ the axial strain at the meeting point of parabolic branch and linear branch

$\varepsilon_y$ the yield strain of steel bars or steel shape

$\theta$ a parameter adopted to assist solving the functions

$\mu$ the frictional coefficient

$\sigma_c$ the axial stress

$\sigma_{cf\theta,p}$ the transverse stress of FRP at peak load

$\sigma_{sh,p}$ the transverse stress of steel tube at peak load

$\sigma_{sh,a}$ the equivalent transverse stress of steel tube

$\sigma_{sv,p}$ the longitudinal stress of steel tube at peak load

# Acknowledgements

The authors gratefully acknowledge the financial support provided by the 13th Five-Year Plan Key R&D Project Topic 1 (2016YFC0701201), National Natural Science Foundation of China (51622802, 51438001), and the financial support from the program of China Scholarship Council (No. 201706050073).

# References

[1] Xiao Y, Wu H. Compressive behavior of concrete confined by carbon fiber composite jackets. J Mater Civil Eng 2000; 12(2):139-46.
[2] Teng JG, Chen JF, Smith ST, Lam L. FRP-strengthened RC structures. UK: John Wiley and Sons, 2002.
[3] Lam L, Teng JG. Design-oriented stress-strain model for FRP-confined concrete. Constr Build Mater 2003; 17(6-7): 471-89.
[4] Wu ZS, Wang X, Iwashita K, Sasaki T, Hamaguchi Y. Tensile fatigue behavior of FRP and hybrid FRP sheets. Compos Part B Eng 2010; 41(5):396-402.
[5] Schneider SP. Axially loaded concrete-filled steel tubes. J Struct Eng 1998; 124(10):1125-38.
[6] de Oliveria WLA, De Nardin S, de Cresce El ALH, El Debs MK. Influence of concrete strength and length/diameter on the axial capacity of CFT columns. J Constr Steel Res 2009; 65(12):2103-10.
[7] Ding FX, Yu ZW, Bai Y, Gong YZ. Elasto-plastic analysis of circular concrete-filled steel tube stub columns. J Constr Steel Res 2011; 67:1567-1577.
[8] Ekmekyapar T, Al-Eliwi BJ. Experimental behaviour of circular concrete filled steel tube columns and design specifications. Thin Walled Struct 2016; 105:220-230.
[9] Kwan AKH, Dong CX, Ho JCM. Axial and lateral stress-strain model for circular concrete-filled steel tubes with external steel confinement. Eng Struct 2016; 117:528-541.
[10] Zhu L, Ma LM, Bai Y, et al. Large diameter concrete-filled high strength steel tubular stub columns under compression. ThinWalled Struct 2016; 108:12-19.
[11] Ouyang Y, Kwan AK. Finite element analysis of square concrete-filled steel tube (CFST) columns under axial compressive load. Eng Struct 2018; 156:443-459.
[12] Wei Y, Jiang C, Wu YF. Confinement effectiveness of circular concrete-filled steel tubular columns under axial compression. J Constr Steel Res 2019; 158:15-27.
[13] Tomii M, Sakino K, Xiao Y, Watanabe K. Earthquake resisting hysteretic behavior of reinforced concrete short columns confined by steel tube. In: Proceedings of the international speciality conference on concrete filled steel tubular structures, Harbin, China; August 1985. P.119-25.
[14] Liu JP, Zhou XH. Behavior and strength of tubed RC stub columns under axial compression. J Constr Steel Res 2010; 66(1):28-36.
[15] Wang XD, Liu JP, Zhang SM. Behavior of short circular tubed-reinforced-concrete columns subjected to eccentric compression. Eng Struct 2015; 105:77-86.
[16] Guo Y, Liu JP, Miao YJ, Wang YH, Xu TX. Experimental study on axial behavior of circular CFRP-steel composite tube confined concrete stub columns. Eng Mech 2017; 34(6):41-50. (In Chinese)
[17] Liu JP, Xu TX, Wang YH, Guo Y. Axial behaviour of circular steel tubed concrete stub columns confined by CFRP materials. Constr Build Mater 2018; 168(4):221-231.
[18] Guo Y, Xu TX, Liu JP. Experimental study and analysis on axial behavior of circular CFRP-steel composite tubed high-strength concrete stub columns. Journal of Building Structures, (In Chinese)
[19] Liu JP, Xu TX, Guo Y, Wang XD, Chen YF. Behavior of circular CFRP-steel composite tubed high-strength concrete columns under axial compression. Steel and Composite Structures,
[20] Ran JH. Axial compression mechanical behavior of FRP-steel composite tube confined concrete stub columns. 2014, Master's thesis, Dalian University of Technology. (In Chinese)
[21] Xiao Y, He WH, Choi K. Confined Concrete-Filled Tubular Columns. ASCE J Struct Eng 2005;

131(3):488-97.
[22] Tao Z, Han LH, Zhuang JP. Axial loading behavior of CFRP strengthened concrete-filled steel tubular stub columns. Adv Struct Eng 2007; 10(1):37-46.
[23] Hu YM, Yu T, Teng JG. FRP-confined circular concrete-filled thin steel tubes under axial compression. ASCE J Compos Constr 2011; 15(5):850-60.
[24] Park JW, Hong YK, Hong GS, Kim JH, Choi SM. Design Formulas of Concrete Filled Circular Steel Tubes Reinforced by Carbon Fiber Reinforced Plastic Sheets. Procedia Eng 2011; 14:2916-22.
[25] Che Y, Wang QL, Shao YB. Compressive performances of the concrete filled circular CFRP-steel tube (C-CFRP-CFST). Adv Steel Constr 2012; 8(4):331-58.
[26] Lu YY, Li N, Li S. Behavior of FRP-confined concrete-filled steel tube columns. Polym 2014; 6(9):1333-49.
[27] Wei Y, Wu G, Li GF. Performance of circular concrete-filled fiber-reinforced polymer-steel composite tube columns under axial compression. J Reinf Compos 2014; 33(20):1911-28.
[28] Li N, Lu YY, Li S, Liu L. Slenderness effects on concrete-filled steel tube columns confined with FRP. J Constr Steel Res 2018; 143:110-18.
[29] Ding FX, Lu DR, Bai Y, Gong YZ, Yu ZW, Ni M, Li W. Behaviour of CFRP-confined concrete-filled circular steel tube stub columns under axial loading. Thin Walled Struct 2018; 125:107-18.
[30] Wang QL, Qu SE, Shao YB, Feng LM. Static behavior of axially compressed circular concrete filled CFRP-steel tubular (C-CF-CFRP-ST) columns with moderate slenderness ratio. Adv Steel Constr 2016; 12(3);263-95.
[31] Wang QL, Zhao Z, Shao YB, Li QL. Static behavior of axially compressed square concrete filled CFRP-steel tubular (S-CF-CFRP-ST) columns with moderate slenderness. Thin Walled Struct 2017; 110:106-22.
[32] Choi K, Xiao Y. Analytical model of circular CFRP confined concrete-filled steel tubular columns under axial compression. ASCE J Compos Constr 2010; 14(1):125-33.
[33] Teng JG, Hu YM, Yu T. Stress-strain model for concrete in FRP-confined steel tubular columns. Eng Struct 2013; 49:156-67.
[34] Dong CX, Kwan AKH, Ho JCM. Axial and lateral stress-strain model for concrete-filled steel tubes with FRP jackets. Eng Struct 2016; 126:365-78.
[35] Yu F, Wu P. Study on stress-strain relationship of FRP-confined Concrete filled steel tubes. Adv Mater Res 2011; 163:3826-29.
[36] Zhang YR, Wei, Y, Bai JW, Zhang YX. Stress-strain model for an FRP-confined concrete filled steel tube under axial compression. Thin Walled Struct 2019; 142:149-159.
[37] EN 1994-1-1 Eurocode 4. Design of Composite Steel and Concrete Structures-Part 1-1: General Rules and Rules for Buildings [S]. Brussels: CEN, 2004.
[38] EN 1992-1-1 Eurocode 2. Design of Concrete Structures-Part 1-1: General Rules and Rules for Buildings [S]. Brussels: CEN, 2004.
[39] GB50010-2010. Code for design of concrete structures; 2002. (In Chinese)
[40] Wang XD. Study on the behavior and strength of TRC and TSRC columns. 2017, Doctor's thesis, Harbin Institute of Technology. (In Chinese)
[41] Baltay P, Gjelsvik A. Coefficient of friction for steel on concrete at high normal stress. J Mater Civil Eng 1990; 2(1):46-49.

[42] Rabbat BG, Russell HG. Friction coefficient of steel on concrete or grout. J Struct Eng 1985; 111(3):505-15.
[43] Pessiki S, Harries KA, Kestner JT, Sause R, Ricles JM. Axial behavior of reinforced concrete columns confined with FRP jackets. ASCE J Compos Constr 2001; 5(4):237-45.
[44] Lam L, Teng JG. Ultimate condition of fiber reinforced polymer-confined concrete. ASCE J compos constr 2004; 8:539-48.
[45] Teng JG, Lam L. Behavior and modeling of fiber reinforced polymer-confined concrete. J Struct Eng 2004; 103:1713-23.
[46] Li SQ, Chen JF, Bisby LA, Hu YM, Teng JG. Strain Efficiency of FRP jackets in FRP-confined concrete-filled circular steel tubes. Int J Struct Stab Dy 2012; 12(1):75-94.
[47] Chen JF. Contribution factors to the reduction of apparent rupture strain in FRP wrapped circular concrete columns. Proceedings of 6th National Conference on FRP in Construction, 11-13(October 2009), Zhengzhou, China (Industrial Construction), 39(433): 15-22.
[48] Lim JC, Ozbakkaloglu T. Confinement model for FRP-confined high-strength concrete. ASCE J Compos Constr 2014; 18(4):04013058.
[49] Mander JB, Priestley MJN, Park R. Theoretical stress-strain model for confined concrete. J Struct Eng 1988; 114(8):1804-26.
[50] Li B, Park R, Tanaka H. Stress-strain behavior of high-strength concrete confined by ultra-high- and normal-strength transverse reinforcements. ACI Struct J 2001; 98(3):395-406.
[51] Xiao QG, Teng JG, Yu T. Behavior and modeling of confined high-strength concrete. J Compos Constr 2010; 14(3):249-59.
[52] Teng JG, Huang YL, Lam L, Ye LP. Theoretical model for fiber-reinforced polymer-confined concrete. J Compos Constr 2007; 11(2): 201-10.
[53] Richart FE, Brandtzaeg A, Brown RL. A study of the failure of concrete under combined compressive stresses. University of Illinois at Urban Champaign, College of Engineering, Engineering Experimental Station, 1928.
[54] Attard MM, Setunge S. Stress-strain relationship of confined and unconfined concrete. ACI Mater J, 1996, 93(5):432-442.
[55] Ozbakkaloglu T, Lim JC, Vincent T. FRP-confined concrete in circular sections: Review and assessment of stress-strain models. Eng Struct 2013; 49:1068-88.
[56] ACI-440.2R(2008). Guide for the Design and Construction of Externally Bonded FRP Systems for Strengthening Concrete Structures, American Concrete Institute, Farmington Hills, Michigan, USA.
[57] Concrete Society (2004). Design Guidance for Strengthening Concrete Structures with Fibre Composite Materials, Second Edition, Concrete Society Technical Report No. 55, Crowthorn, Berkshire, UK.
[58] Popovics S. A numerical approach to the complete stress-strain curves for concrete [J]. Cement Concrete Res 1973; 3(5):583-99.